The Flux and Provenance of Dust Delivered to the SW Pacific During the Last Glacial Maximum

M. D. Trudgill[1,2] (iD), R. Shuttleworth[1] (iD), H. C. Bostock[3,4] (iD), A. Burke[2] (iD), M. J. Cooper[1] (iD), R. Greenop[2] (iD), and G. L. Foster[1] (iD)

[1]School of Ocean and Earth Science, National Oceanography Centre, University of Southampton, Southampton, UK, [2]Department of Earth and Environmental Sciences, University of St Andrews, St Andrews, UK, [3]National Institute of Water and Atmospheric Research, Wellington, New Zealand, [4]School of Earth and Environmental Sciences, University of Queensland, Brisbane, Queensland, Australia

Abstract Atmospheric dust is a primary source of iron (Fe) to the open ocean, and its flux is particularly important in the high nutrient, low chlorophyll (HNLC) Southern Ocean where Fe currently limits productivity. Alleviation of this Fe limitation in the Subantarctic Zone of the Atlantic by increased dust-borne Fe supply during glacial periods has been shown to increase primary productivity. However, previous work has found no such increase in productivity in the Pacific sector. In order to constrain the relative importance of Southern Ocean Fe fertilization on glacial-interglacial carbon cycles, records of dust fluxes outside of the Atlantic sector of the Southern Ocean at the Last Glacial Maximum (LGM) are required. Here we use grain size and U-series analyses to reconstruct lithogenic and $CaCO_3$ fluxes and Nd, Sr, and Pb isotopes to ascertain the provenance of terrigenous material delivered to four deep water cores in the SW Pacific Ocean over the last ~30 kyr. We find evidence for an increase in the relative proportion of fine-grained (0.5–12 μm) terrigenous sediment and higher detrital fluxes during the LGM compared to the Holocene. The provenance of the LGM dust varied spatially, with an older, more "continental" signature (low ε_{Nd}, high $^{87}Sr/^{86}Sr$) sourced from Australia in the northern cores, and a younger, more volcanogenic source in the southern cores (high ε_{Nd}, low $^{87}Sr/^{86}Sr$), likely sourced locally from New Zealand. Given this increase in lithogenic flux to the HNLC subantarctic Pacific Southern Ocean during the LGM, factors besides Fe supply must have regulated the biological productivity here.

1. Introduction

An 80–100 ppm change in atmospheric CO_2 is observed during late Pleistocene glacial-interglacial cycles (Bereiter et al., 2015), with numerous lines of evidence pointing toward a mechanism that involves a change in the size of the deep ocean carbon reservoir (e.g., Archer et al., 2000; Kohfeld & Ridgwell, 2009). One such mechanism thought to play an important role is the iron (Fe) fertilization hypothesis (Martin et al., 1994). The lack of this important micronutrient limits primary productivity in High Nutrient Low Chlorophyll (HNLC) regions of the ocean today, in particular the Southern Ocean (Martin et al., 1994). An enhanced supply of dust-borne Fe to the Southern Ocean during glacial periods would stimulate productivity, strengthening the biological pump and drawing down atmospheric CO_2 (Martin et al., 1994). While increased productivity is observed in the Atlantic sector of the Southern Ocean associated with increased Fe flux (Martínez-García et al., 2014), no such change in productivity is observed in other sectors of the Southern Ocean, such as the SW Pacific (Chase et al., 2003; Durand et al., 2017). However, it remains unclear if this lack of increased primary productivity during the Last Glacial Maximum (LGM) in this region is attributable to a diminished dust input or other limiting factors.

Supply of the micronutrient Fe to the Southern Ocean is thought to have increased during the LGM (De Angelis et al., 1987; Kumar et al., 1995). Dust is a dominant external source of Fe to the open ocean (Jickells et al., 2005), although there is a growing body of literature surrounding the importance of glaciers in providing bioavailable Fe to near coastal environments (Bhatia et al., 2013; Hawkings et al., 2014, 2018), and recent work has suggested that upwelling, hydrothermal activity, and resuspension of sediments on continental shelves also represent significant Fe sources (Ardyna et al., 2019; Tagliabue et al., 2017). Dust supply increased during glacial periods through a number of processes linked to a weakened hydrological cycle, enhanced aridity, and increased wind strength and gustiness (Mahowald et al., 2005; McGee et al., 2010;

Table 1
Summary of Cores Used in This Study

	Latitude	Longitude	Water depth (m)	Water mass	Average sedimentation rate (cm/kyr)	Age model
P71	33°51′18.0″S	174°41′36.0″E	1,919	STW	1.12	Duncan et al. (2016)
MD97-2121	40°22′56.1″S	177°59′40.8″E	2,314	STW	37.09	Carter et al. (2008)
TAN1106-28	48°22′19.2 S	165°39′32.4″E	2,798	STF	7.34	Bostock et al. (2015)
TAN1106-43	50°26′56.4″S	164°52′40.8″E	3,670	SAW	6.66	Bostock et al. (2015)

Note. Water masses are subtropical waters (STW), subtropical front (STF), and subantarctic waters (SAW).

Winckler et al., 2008). First, a decrease in global mean rainfall led to a decline in vegetation and the expansion of deserts, while strengthened winds increased the entrainment of fine sediment particles (Mahowald et al., 2005; Werner et al., 2002; Winckler et al., 2008). Second, an increased temperature gradient between the pole and the equator during the glacial period led to an increase in wind gustiness, which in turn may have led to increased dust emissions (McGee et al., 2010). Third, increased glacial activity resulted in an increased supply of dust from easily mobilized fine grained material from glacial outwash plains (Bullard et al., 2016; Delmonte et al., 2017; Lamy et al., 2014; Marx et al., 2018; Shoenfelt et al., 2018; Sugden et al., 2009) which can also be transported in glacial runoff to the open ocean (Bhatia et al., 2013; Hawkings et al., 2014, 2018). This glacially derived Fe is thought to be more bioavailable than Fe in lithogenic material produced by arid weathering regimes, as it has undergone less chemical weathering so comprises more leachable, bioavailable Fe (II) (Hawkings et al., 2018; Schroth et al., 2009; Shoenfelt et al., 2017, 2019).

Three major dust source regions have previously been proposed for the Southern Ocean in atmospheric transport models: South America, South Africa, and Australia (Albani et al., 2012; Lamy et al., 2014; Li et al., 2008). In these models, the SW Pacific region is predominantly influenced by an Australian source of dust (Albani et al., 2012; Lamy et al., 2014; Li et al., 2008). Indeed, there is evidence for Australian dust making it to Antarctica during the Holocene (Aarons et al., 2017; De Deckker, 2019). Although New Zealand is often not considered a major dust source region in most model simulations, when dust trajectories are considered, it is apparent that dust produced in New Zealand is widely dispersed (Neff & Bertler, 2015). Models all show an increase in dust flux to the SW Pacific at the LGM compared to the Holocene. However, the magnitude of this difference varies between models. Mahowald et al. (2006) and Werner et al. (2002) find relatively small differences between the LGM and Holocene (between 1 and 4 times larger at the LGM), whereas Albani et al. (2012) find fluxes that are up to 9 times higher at the LGM. The absolute fluxes in SW Pacific also vary between the models by an order of magnitude (Albani et al., 2012; Mahowald et al., 2006; Werner et al., 2002).

This study combines records of lithogenic fluxes, carbonate productivity, and sediment provenance to determine the extent to which increased glacial supply of the micronutrient Fe increased biological productivity in the SW Pacific, a region where few estimates currently exist. To this end, we analyzed the abundance of fine grained lithogenic material (0.5–12 μm particle diameter, mean 1.8 μm), the sediment isotopic composition, and the flux of $CaCO_3$ in four cores from the SW Pacific sector of the Southern Ocean during the Holocene and LGM (30 ka to present, Table 1 and Figure 1). The four cores form a transect from subtropical waters in the north (33°S) to subantarctic waters in the south (50°S; Figure 1). Previous records of dust flux changes between the LGM and Holocene show higher fluxes at the LGM at a regional scale (Hesse, 1994; Hesse & McTainsh, 1999; Thiede, 1979). However, south of New Zealand within the Subantarctic Zone, data are scarce (Durand et al., 2017; Hesse, 1994; Hesse & McTainsh, 1999; Kohfeld et al., 2013; Thiede, 1979), and the only constraints on the provenance of the dust in this region are limited to surface sediments (Graham et al., 1997; Marx et al., 2005; Molina-Kescher et al., 2014; Wengler et al., 2019). We first quantified the proportion of different grain size end members in the bulk sediment by end member modeling to define and quantify the proportion of fine grained (0.5–12 μm particle diameter, mean 1.8 μm) lithogenic material present. This is similar to previous dust size ranges for this region and across the Pacific from Rea (1994). Due to the proximal location of our cores to New Zealand, this fine-grained material is likely a combination of fluvially delivered material and atmospherically delivered dust, but regardless of its mode of transport, it
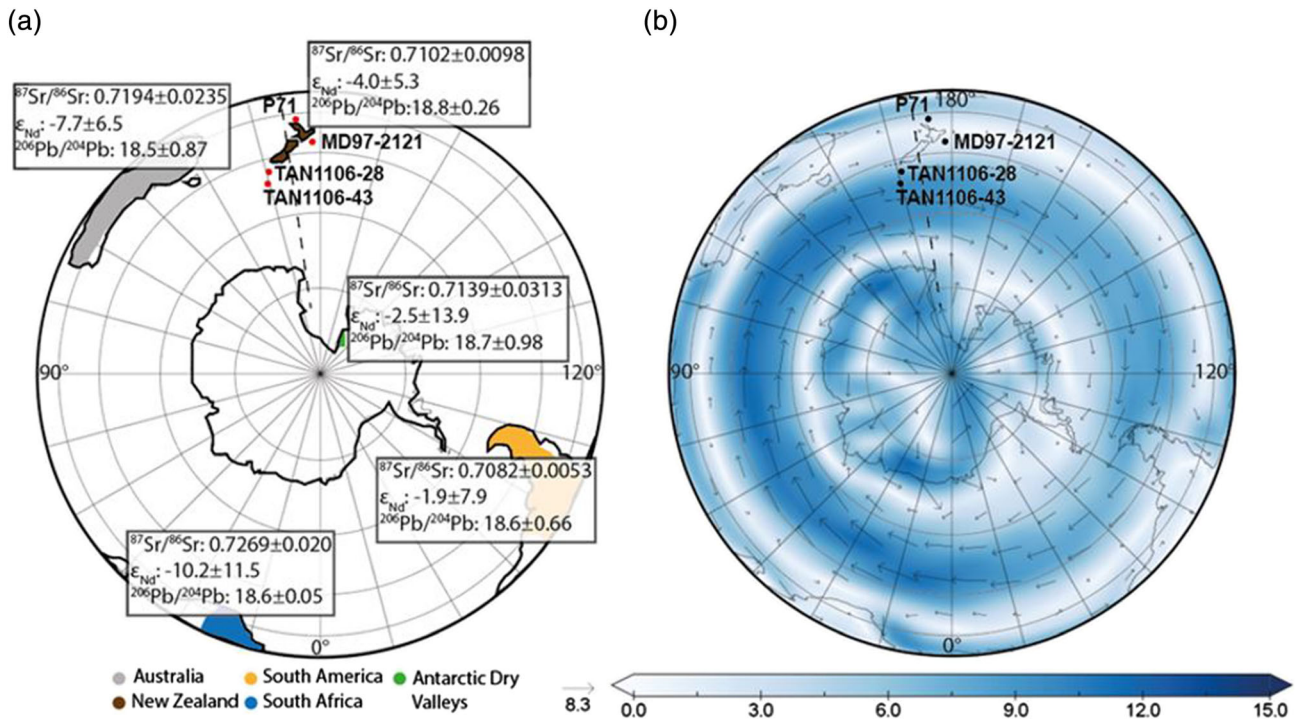
Figure 1. Major dust source locations and wind vectors across the Southern Ocean. (a) Sr, Nd, and Pb isotopic compositions of major Southern Hemisphere dust sources shown by mean value $\pm$ 2σ. (b) Average January surface wind vectors (black arrows) and speeds (blue shading, darker colors represent higher wind speeds) relative to location of cores used in this study. Average isotope values for source regions after Basile et al. (1997, 2001), Blakowski et al. (2016), Delmonte et al. (2004a), Gili et al. (2016, 2017), Grousset et al. (1992), Pichat et al. (2014), Revel-Rolland et al. (2006), Vallelonga et al. (2010), and references therein. Wind vector data set from http://www.esrl.noaa.gov/psd, Kalnay et al. (1996). Dust source region shapes based on Basile et al. (1997). Latitudinal transect of Figure 6 shown by dashed line.

remains a potential source of Fe to the currently Fe-limited surface water. We estimated the total detrital and dust flux and $CaCO_3$ flux (a proxy of productivity) using uranium series isotopes and thorium normalization to remove the effects of lateral sediment transport on the seafloor (Costa et al., 2020; Henderson & Anderson, 2003; McGee et al., 2007). Finally, changes in the provenance of the sediment were determined by comparing their neodymium (Nd), strontium (Sr), and lead (Pb) isotopic composition with previous studies from potential dust source regions around the Southern Hemisphere (Figure 1, e.g., Delmonte et al., 2004a; Vallelonga et al., 2010), determining the changing source of lithogenic fluxes to the SW Pacific over the last 30 kyr.

2. Materials and Methods

2.1. Core Location, Sampling, and Grain Size Analysis

Samples were collected from the following cores: P71, MD97-2121, TAN1106-28, and TAN1106-43 (Table 1 and Figure 1), which form a latitudinal transect from 33–50°S. The cores had significantly different sedimentation rates (Table 1) and the number of samples analyzed varied by technique (for numbers; see Table S1 in the supporting information). The age models of cores TAN1106-28 and TAN1106-43 are based on tuning the deglacial trends observed in the $\delta^{18}O_{G.bulloides}$ record to the Lisiecki and Raymo (2005) benthic stack and are complemented by three radiocarbon ages in each core measured on a mixed planktic foraminifera assemblage (Bostock et al., 2015). Core P71's age model is based on comparison of the $\delta^{18}O_{U. peregrina}$ to the Lisiecki and Raymo (2005) benthic stack (Duncan et al., 2016). The core chronology for MD97-2121 is based on 9 tephra dates and 20 Accelerator Mass Spectrometry (AMS) ^{14}C dates of planktic foraminifera of mixed assemblage (Carter et al., 2008). For cores MD97-2121, TAN1106-43, and P71, Holocene and LGM age, we used freeze dried <63 μm sediment samples, which had been previously separated by sieving.

Additionally, a time series of freeze-dried bulk sediment from TAN1106-28 was taken every ~5 kyr from 2–17 ka and every ~2 kyr from 17–25 ka. In the time series from TAN1106-28, samples are classified based on age as Holocene (<12 ka), deglacial (12–18 ka), LGM (18–27 ka), and glacial (>27 ka).

The grain size of the <63 μm fraction of sediment for the cores TAN1106-28, TAN1106-43, and MD97-2121 was analyzed by laser diffraction using the Coulter LS130 at the University of Southampton. Samples were decarbonated by leaching in 10% acetic acid overnight (Organic carbon content of the samples was very low [<1%] and assumed to be minimal in these samples; opal content was low [<5%] and not removed but may have had a small influence on grain size distributions, as discussed below; Bostock et al., 2019; Carter & Manighetti, 2006). Samples were disaggregated prior to analysis using Calgon solution (5%) at a ratio of 1:10 (Calgon: sample; Blott et al., 2004). Three replicates were taken for each sample, and the arithmetic mean was taken and used in all subsequent data analysis. For grain size analysis, either freeze dried <63 μm (MD97-2121 and TAN1106-28) or wet bulk sediment (TAN1106-43 and TAN1106-28) was used. Where bulk sediment was used, only the <63 μm component was used to calculate relative proportions.

End member analysis was performed on the <63 μm component using the AnalySize software in MATLAB (version 1.1.0, Paterson & Heslop, 2015). End members were fitted parametrically with a General Weibull distribution. To evaluate the number of end members in the grain size distributions, 1–10 end members were fitted to the data set as a whole. The coefficient of determination (R^2) and angular deviation for each of these fits were assessed to determine how many end members best describe the data.

2.2. Isotopic Analysis

Bulk sample digest and analyses of Sr, Nd, and Pb were undertaken in clean chemistry laboratories (Class 100) at the University of Southampton. Nitric and hydrochloric acids used in sample preparation were purified by subboiling distillation using Savillex DST-1000 Teflon stills. Approximately 75 mg of sediment for each sample was digested on a hot plate using Savillex Teflon vials that had been acid cleaned in hot 50% HCl and hot 50% HNO_3 overnight. First, 5 ml of aqua regia freshly prepared from subboiled acids was added and left overnight to remove reactive organics. This was followed by dissolution in a 2.5 ml HNO_3, 3 ml HF (Romil SpA grade) mix. Finally, 2 ml $HClO_4$ (Fisher Trace element grade) was added and samples were completely dried down again. They were then redissolved in 10 ml of 6 M HCl. The concentrations of Pb, Sr, and Nd were determined on a ThermoFisher Scientific XSeries2 ICP-MS at the University of Southampton on diluted subsamples using synthetic standards to calibrate. Based on the concentration results, the bulk sample was split into separate subsamples that contained at least 300 ng Pb, 1 μg Sr, and 200 ng Nd which were dried down prior to column chemistry. For the U-series analyses, a final subsample representing approximately 15 mg of original sediment (~ 20%) was taken.

2.2.1. Strontium

Strontium (Sr) was separated using ~50 μl TrisKem Sr Resin columns with a 3 M HNO_3 elution acid (Lang et al., 2014). High levels of barium in some samples caused poor recovery and/or poor ionization. These samples were rerun from the bulk digest using the same method but using 8 M HNO_3 as the eluant.

The dried down samples were loaded onto tantalum (Ta) filaments with a Ta activator solution and measured on the ThermoScientific Triton Plus thermal ionization mass spectrometer (TIMS) at the University of Southampton, using a static procedure with amplifier rotation with an ^{88}Sr beam of ~2 V. Fractionation was corrected using an exponential correction (Russel et al., 1978) normalized to ^{86}Sr/^{88}Sr = 0.1194 (Nier, 1938). NIST 987 (0.710249; Yobregat et al., 2017) was run as a reference standard, and its long-term average on this instrument is 0.710249 ± 0.000022 (2σ) on 70 analyses. Analysis of the BHVO2 reference material using the same column procedure gave 0.703476 ± 0.000012 (2SE) compared to the expected value 0.703478 ± 0.000034 (1sd) from the GeoReM database (Jochum et al., 2007).

2.2.2. Neodymium

Neodymium (Nd) was separated using a two column procedure modified from Scher and Delaney (2010): first, a 200 μl Bio-Rad AG50 X8 (200–400 mesh) was used to isolate the REE from the major cations, and then a 300 μl TrisKem Ln resin (50–100 μm) was used to isolate the Nd, eluting with 0.25 M HCl. The final collected fractions were dried down and redissolved in 3% HNO_3 to give a Nd concentration of 50 ppb and were measured on a ThermoScientific Neptune multicollector inductively coupled plasma mass spectrometer (MC-ICPMS) at the University of Southampton. The method is based on Vance and Thirlwall (2002)

through adjustment to a ^{146}Nd/^{144}Nd ratio of 0.7219 and a secondary normalization to ^{142}Nd/^{144}Nd = 1.141876. Measurements of the JNdi-1 reference standard (0.512115 ± 0.000007; Tanaka et al., 2000) gave ^{143}Nd/^{144}Nd ratio of 0.512115 ± 0.000006 (2σ) across six analysis sessions over a 2 year period. BHVO2 through the same chemistry procedure gave 0.512999 ± 0.000006 (2SE) compared to the expected value of 0.512979 ± 0.000014 (1sd) from GeoRem database (Jochum et al., 2007). These ratios are reported relative to the ^{143}Nd/^{144}Nd ratio of the chondritic uniform reservoir (CHUR, 0.512638, Jacobsen & Wasserburg, 1980) using the epsilon notation:

$$\varepsilon_{Nd} = \left[\frac{\left(\frac{^{143}Nd}{^{144}Nd}\right)_{sample}}{\left(\frac{^{143}Nd}{^{144}Nd}\right)_{CHUR}} - 1 \right] \times 10,000 \tag{1}$$

2.2.3. Lead
The lead (Pb) was isolated using a column of precleaned Bio-Rad AG-1 X8 (200–400 mesh) using HBr and HCl to elute (Brown et al., 2020). The collected fractions were dried down before being redissolved in 3% HNO_3. The sample was split into two fractions to give a final concentration of 20 ppb in each. One fraction was run unspiked, while the other was spiked with the SBL74 double spike (Taylor et al., 2015) to allow correction of instrumental mass fractionation. The natural and double spiked fractions were run during separate analytical sessions on the ThermoScientific Neptune MC-ICPMS at the University of Southampton. NIST981 was run during the analyses and the long-term averages for the method are ^{206}Pb/^{204}Pb 16.94 ± 0.0023 (2σ), ^{207}Pb/^{204}Pb 15.496 ± 0.0026 (2σ), and ^{208}Pb/^{204}Pb 36.7124 ± 0.0076 (2σ) on >100 analyses compared to the defined values of ^{206}Pb/^{204}Pb 16.9412 ± 0.0003 (2σ), ^{207}Pb/^{204}Pb 15.4988 ± 0.0006 (2σ), and ^{208}Pb/^{204}Pb 36.7233 ± 0.0013 (2σ) (Taylor et al., 2015).

2.2.4. U-Series
The U-series subsample was spiked with a mixed ^{236}U-^{229}Th standard in the STAiG Labs at the University of St Andrews. The Th and U fractions were separated on 500 µl UTEVA resin columns (Nita, 2012). The dried down fractions were taken up in 2% HCl and analyzed using a Neptune Plus MC-ICPMS at the University of St Andrews following the procedure outlined in Hoffmann et al. (2007) to determine the ^{230}Th, ^{232}Th, ^{234}U, and ^{238}U activities. External reproducibility of the ^{230}Th, ^{232}Th, ^{234}U, and ^{238}U activities on two complete replicates was <1.5%.

2.3. Source Region Compilation

A compilation of the Sr, Nd, and Pb isotopic compositions of the major dust source regions in the Southern Hemisphere was compiled from Basile et al. (1997, 2001), Blakowski et al. (2016), Delmonte et al. (2004a), Gili et al. (2016, 2017), Grousset et al. (1992), Pichat et al. (2014), Revel-Rolland et al. (2006), Vallelonga et al. (2010), and references therein. These data represent the Sr, Nd, and Pb isotopic compositions of the <5 µm or bulk fraction of aeolian dust deposits and material in regions determined to be sources of atmospheric dust in the present day and/or at the LGM taken from dried lake beds, loess, and regolith deposits, glacial drift, and suspended dust captured directly from dust storms (summarized in Figure 1).

3. Results

3.1. Grain Size Distribution

The grain size distributions for all samples show a polymodal distribution with a modal peak around 9 µm (Figure 2). The parametric fitting of the grain size distributions with a General Weibull distribution assuming from 1–10 end members shows that the coefficient of determination (R^2) and angular deviation reach a plateau at three end members, suggesting that a three end member model best describes the data. With three end members, R^2 values are typically above 0.9, with the lowest value (0.77) from 219–220 cm in TAN1106-28 (Figure S1 and Table S2). Thus, three end members were modeled for all sites and time periods.

The finest (End Member 1) has a mean particle diameter of 1.8 µm and is interpreted to be atmospheric dust (Maher et al., 2010; Rea, 1994), with the caveat that due to the proximal nature of our cores it may also contain a fluvial contribution. Although the patterns are broadly similar between the Holocene and LGM, the proportion of EM1 of 6.6% in MD97-2121, 10.1% in TAN1106-43, and 14.9% in TAN1106-28 was proportionally higher at the LGM relative to the Holocene. End Member 2 has a mean particle diameter of 9.4 µm. The
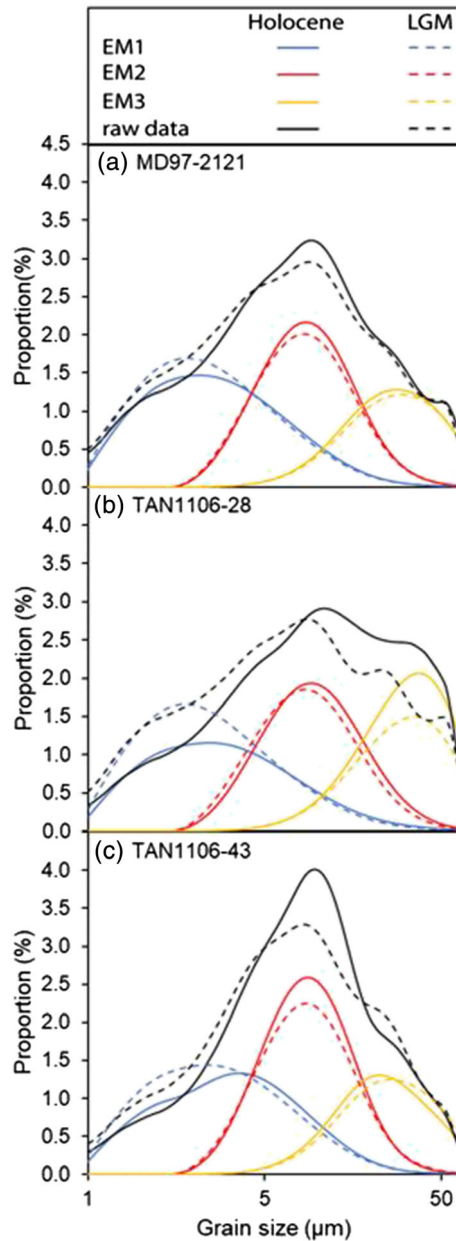
Figure 2. (a–c) Grain size and end member (EM) distributions of <63 μm fraction of sediment. Average grain size distribution of <63 μm fraction of cores TAN1106-43, TAN1106-28, and MD97-2121 for Holocene (0–12 ka, solid) and LGM (18–27 ka, dashed) age samples.

larger mean particle diameter observed in End Member 2 represents the primary grain size fraction in the cores studied, averaging 47% of the <63 μm material. In all the cores we studied the proportion of material in End Member 2 is lower at the LGM, by 6.6%, 13.5%, and 5.6% for MD97-2121, TAN1106-43, and TAN1106-28, respectively. This fraction is interpreted to be of fluvial origin. There is also a third end member which displays a variable peak with a median particle size of 39 μm. This third end member shows no difference on average between LGM and Holocene age samples in MD97-2121 and TAN1106-43, but in TAN1106-28 it represents 9.3% more of the total sample in Holocene age samples than in LGM age samples. The <63 μm fraction measured here represents most of the sediment from these cores (~93% average).

Opal was not removed from these samples prior to grain size analysis as it represents a low proportion of material in the cores studied (<5%, Bostock et al., 2019; Carter & Manighetti, 2006), and either shows no trend through time or a slight increase in the deglacial (Bostock et al., 2019; Carter & Manighetti, 2006). Diatoms are typically in the 10–50 μm size fraction (Pugh & McCave, 2011) so would contribute to either End Member 2 or 3. To check if changes in opal content affect our grain size records, we calculated the proportion of opal in each sample after the carbonate fraction was removed and then used these to recalculate the End Member 1 proportion and flux assuming the diatoms contributed to End Member 2 or 3 (Figure S2). These analyses show very little change in pattern or value from our initial results, indicating that opal had little impact on the interpretation of our grain size records.

3.2. ^{232}Th Flux and CaCO$_3$ Flux

^{230}Th is produced by decay of ^{234}U in the ocean at a constant rate and immediately adsorbed onto settling particles (Henderson & Anderson, 2003). The ratio of the activity of this scavenged ^{230}Th to the theoretical production rate of ^{230}Th in the water column gives the vertical flux of material, and multiplying by the measured ^{232}Th (assumed to be entirely continentally derived) yields a proxy for the flux of continental material. This ^{232}Th flux can then be converted to a detrital flux by assuming a 10.7 ppm concentration of ^{232}Th in any continental material delivered (McGee et al., 2007; Taylor & McLennan, 1985). This continental material is a combination of dust delivered to the ocean atmospherically and sediments transported fluvially. This detrital flux, determined from ^{232}Th flux, was higher at MD97-2121, TAN1106-28, and TAN1106-43 during the LGM than during the Holocene (Figure 3b). Little change was observed at P71; however, this site was sampled slightly before the LGM, due to the low sedimentation rates in this core (Table 1) and changes are small enough to be considered within error (0.2 g/m^2/year lower during the glacial than during the Holocene). Multiplying these detrital fluxes by the proportion of material in each end member gives an estimate of their flux:

$$End\ member\ flux = \frac{\beta \times z}{^{230}Th^0_{scavenged}} \times {}^{232}Th_{measured} \times {}^{232}Th_{average\ continental} \times End\ member\ proportion \quad (2)$$

where β is the production rate of ^{230}Th in the water column (β = 0.0267 dpm m^{-3} year^{-1}, Henderson & Anderson, 2003) and z is water depth (m). ^{230}Th$^0_{scavenged}$, the original activity of ^{230}Th produced by the decay of ^{234}U and scavenged onto sinking particles, is determined by calculating the activity of ^{230}Th produced by other sources (authigenic and detrital, for further details see Costa et al., 2020; Henderson &
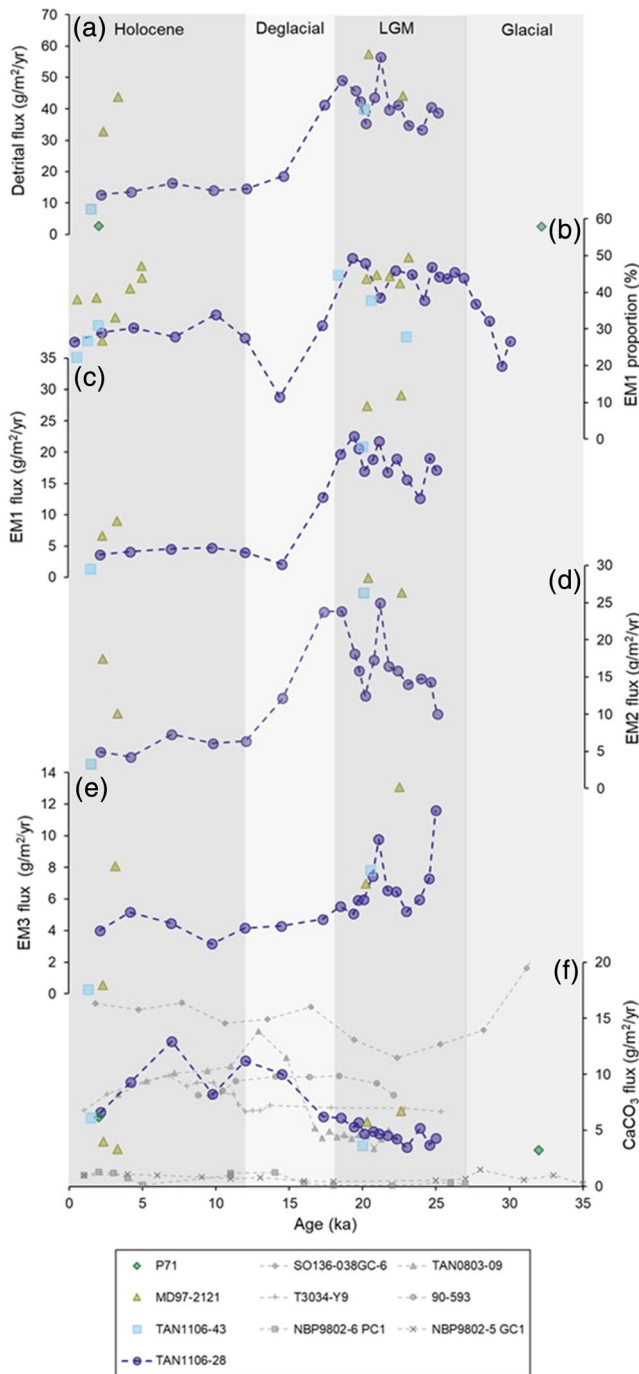
Figure 3. Detrital flux (from ^{232}Th fluxes), proportion of material in End Member 1 (EM1) in the lithogenic fraction of sediment, the fluxes of End Members 1–3 (EM1, EM2, and EM3) through time, and CaCO$_3$ flux with respect to time. (a) Detrital flux; calculated from ^{232}Th fluxes, normalized using ^{230}Th to correct for potential sediment focusing. (b) Proportion of material in End Member 1 (see Figure 2). (c–e) Flux of End Members 1, 2, and 3 through time; calculated by multiplying the proportion of material in each end member by the detrital flux (Equation 2). (f) ^{230}Th normalized CaCO$_3$ flux, calculated by multiplying the %CaCO$_3$ (Bostock et al., 2015; Carter & Manighetti, 2006; Duncan et al., 2016) by the ^{230}Th normalized vertical flux of material. Measurements for other cores are shown in gray (Chase et al., 2003; Durand et al., 2017), all core locations shown in Figure S3.

Anderson, 2003), subtracting them from the measured ^{230}Th activity and correcting for decay of ^{230}Th since deposition. Although proportionally there are variations between the different end members through time, the fluxes of all three decrease during the deglacial (Figure 3), though most strongly in End Member 1, as it proportionally also decreases during the deglacial. The flux of End Member 1 is higher at the LGM than in the Holocene by 20.5 g/m^2/year in MD97-2121, by 14.1 g/m^2/year in TAN1106-28 and by 17.3 g/m^2/year in TAN1106-3 (Figure 3).

We can also use our ^{230}Th normalized burial flux to reconstruct CaCO$_3$ flux by multiplying it by published records of %CaCO$_3$ (Bostock et al., 2015; Carter & Manighetti, 2006; Duncan et al., 2016) using the equation:

$$CaCO_3\ flux = \frac{\beta \times z}{^{230}Th^0_{scavenged}} \times \%CaCO_3 \tag{3}$$

CaCO$_3$ flux has been used extensively in other studies as a proxy for productivity in this region (Carter et al., 2000; Chase et al., 2003; Durand et al., 2017). Although in some regions it can reflect a dissolution signal, around New Zealand it is in agreement with other records of palaeo-productivity (C$_{org}$, excess Ba and opal mass accumulation rates, Zn/Si ratios of sponge spicules; Carter et al., 2000; Chase et al., 2003; Durand et al., 2017; Ellwood et al., 2005). In TAN1106-28, TAN1106-43, and P71, CaCO$_3$ fluxes show an increase from the glacial into the Holocene from 4.7 to 9.6, 3.7 to 6.1 and 3.2 to 6.2 g/m^2/year, respectively (Figure 3). In contrast, in MD97-2121 there is a decrease in CaCO$_3$ flux from the LGM to Holocene from 6.2 to 3.7 g/m^2/year (Figure 3).

3.3. Provenance

Pb, Nd, and Sr isotopic composition of the <63 μm fraction of sediment varies between the LGM and Holocene in all four cores examined in this study. In cores MD97-2121 and P71, the ^{87}Sr/^{86}Sr ratio is slightly higher at the LGM (0.70965 and 0.70908) compared to the Holocene (0.70960 and 0.70906, respectively) and ε$_{Nd}$ is slightly more negative in the LGM (−3.80 and −2.48) compared to the Holocene (−3.45 and −2.23, respectively) (Figure 4). In TAN1106-28 and TAN1106-43 the opposite occurs, and glacial samples have a lower ^{87}Sr/^{86}Sr ratio (0.70819 and 0.70861 average at the LGM vs 0.70870 and 0.709073 average in the Holocene for each core, respectively) and more positive ε$_{Nd}$ values (−4.44 and −4.37 average at the LGM vs. −4.79 and −5.22 average in the Holocene for each core respectively, Figure 4). Note that for both TAN cores, this change is significantly larger compared to the two northern cores (the difference between glacial and interglacial Sr ratios is 13 times larger, and the difference in ε$_{Nd}$ values is 2 times larger in TAN cores than the two northern cores).

4. Discussion

4.1. Sources of Different End Members

We find evidence for three end members in our grain size distributions (Figure 2). Long traveled atmospheric dust is typically fine grained (between 1.5 and 3 μm, e.g., Delmonte et al., 2004b; Maher et al., 2010), whereas more proximal dust is coarser grained, clustering around 5 μm (Maher et al., 2010), and in some cases is much coarser (e.g., 20–50 μm; Muhs et al., 2007). Indeed, grain size analysis on sediment cores in the
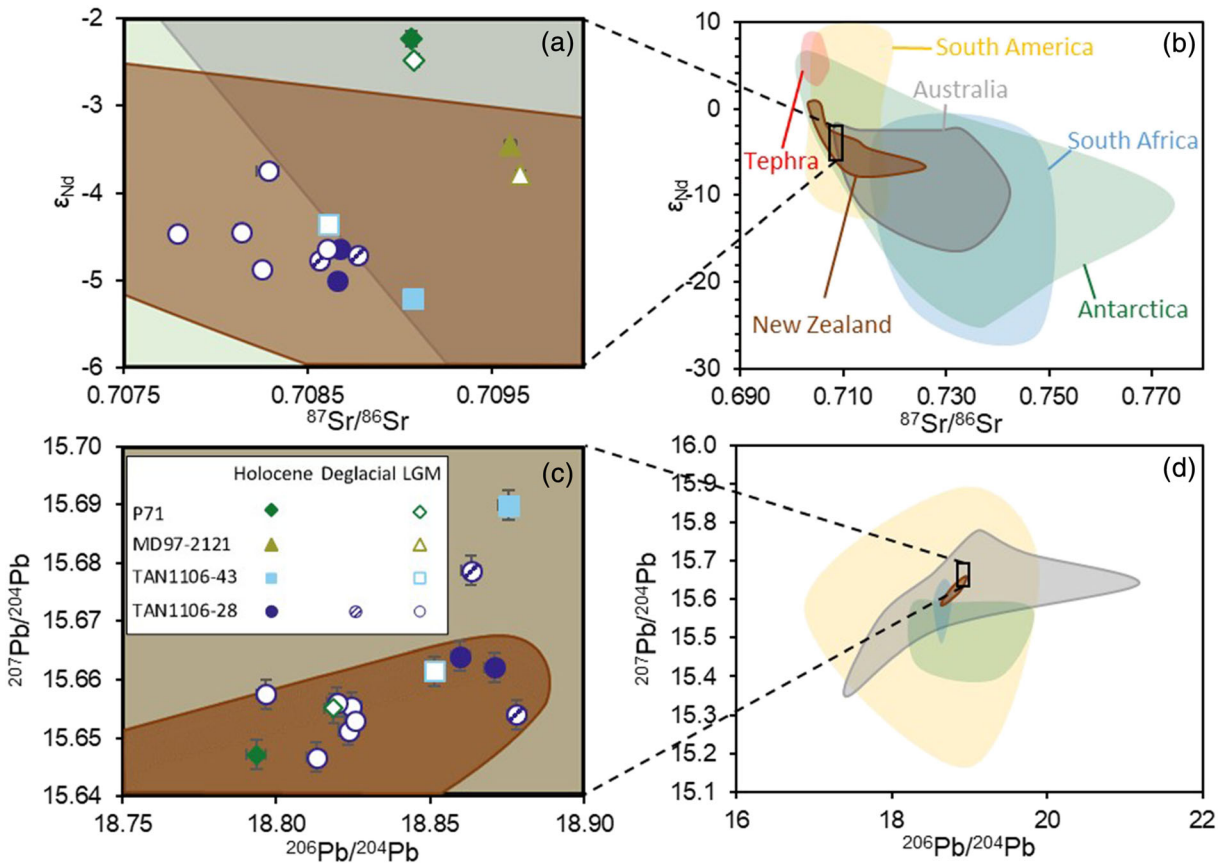
Figure 4. (a, b) $^{87}Sr/^{86}Sr$, ε_{Nd} and (c, d) $^{207}Pb/^{204}Pb$ and $^{206}Pb/^{204}Pb$ isotope changes through time in TAN1106-28 (dark blue circles), TAN1106-43 (light blue squares), MD97-2121 (light green triangles), and P71 (dark green diamonds) compared to Southern Hemisphere potential dust source areas: Australia (gray), New Zealand (brown), South Africa (blue), Antarctic dry valleys (green), and South America (yellow), compiled from Basile et al. (1997, 2001), Blakowski et al. (2016), Delmonte et al. (2004a), Gili et al. (2016, 2017), Grousset et al. (1992), Pichat et al. (2014), Revel-Rolland et al. (2006), Vallelonga et al. (2010), and references therein. Holocene ages samples shown by infilled symbols, deglacial by hatched symbols, and LGM by empty symbols. Errors shown are the larger value of the internal or external measured error; where not shown, error is smaller than symbol size.

Tasman Sea and the Pacific ocean find a dust mode in this region with a peak between 2 and 4 μm (Hesse & McTainsh, 1999; Rea, 1994), with a second dust mode found in the Tasman Sea with peak around 19–23 μm (Hesse & McTainsh, 1999). Estimates of the grain size of fluvial sediment find a median grain size between 6.1 and 9.1 μm in Fiordland, the closest region of New Zealand to TAN1106-28 and TAN1106-43 (Ramirez et al., 2016), and similar grain size estimates, or coarser, are measured and modeled for other coastal regions around New Zealand (Haddadchi et al., 2017). We therefore attribute our End Member 1 (0.5–12.5 μm, modal diameter 1.8 μm) to atmospheric dust. End Member 2 (2.7–33.9 μm, modal diameter 9.5 μm) fits the grain size of fluvial sediments from New Zealand and could also include the second coarser dust peak from the Tasman Sea. As the grain size better fits the range found for fluvial sediments, it seems likely that this end member is largely fluvially derived, though may have a small dust component. End Member 3 (10.4–64.2 μm, modal diameter 38.9 μm) could also include this second dust peak or could be fluvially sourced. As End Member 1 is the only end member we can confidently attribute to be dust we use the flux of End Member 1 through time as a proxy for dust flux. However, all three end member fluxes show similar trends through time, with higher fluxes in the glacial compared to the Holocene, so any uncertainty surrounding the attribution of a dust end member has little impact on our interpretations.

4.2. Pb-Nd-Sr Evidence for Spatial Variations in Dust Sources

The sediment from the LGM in these cores is characterized by a higher detrital flux with a greater proportion of the fine grained End Member 1 (Figures 3 and 5) relative to the Holocene. These observations are indicative of an LGM-aged increase in the supply of atmospheric dust or fine-grained material from glacial
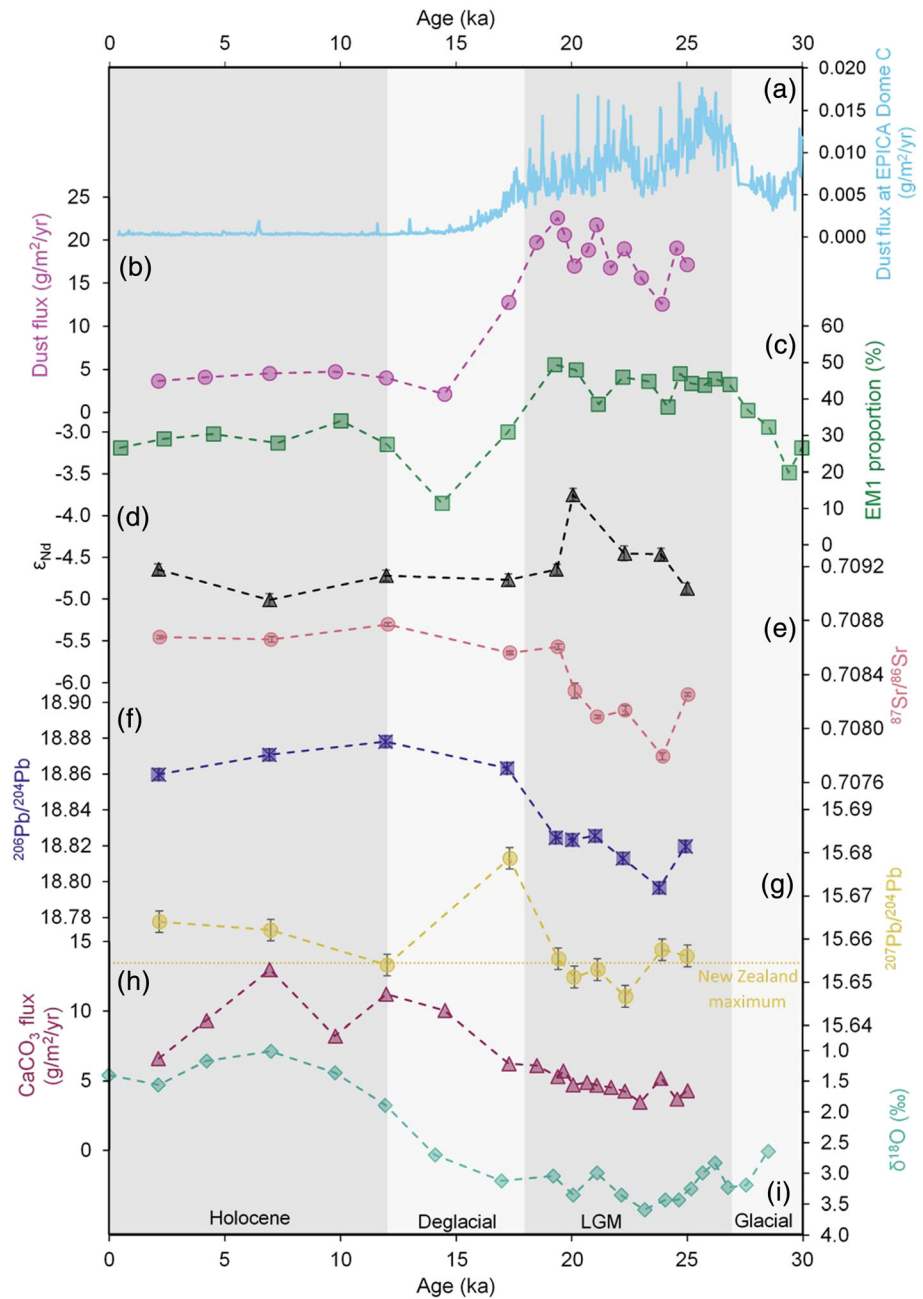
Figure 5. (a) Dust flux at EPICA Dome C (Lambert et al., 2012) compared to sedimentary records from TAN1106-28 (b–i). (b) Dust flux (calculated from detrital flux multiplied by the proportion of sediment in EM1). (c) Proportion of material in End Member 1 (EM1). (d) ε_{Nd}. (e) $^{87}Sr/^{86}Sr$. (f) $^{206}Pb/^{204}Pb$. (g) $^{207}Pb/^{204}Pb$ with the maximum source region value measured for New Zealand indicated by a dotted line (Vallelonga et al., 2010), maximum values for ε_{Nd}, $^{87}Sr/^{86}Sr$, and $^{206}Pb/^{204}Pb$ are well above those measured here for New Zealand and Australia. (h) ^{230}Th normalized $CaCO_3$ flux (g/m^2/yr); %$CaCO_3$ (Bostock et al., 2015) multiplied by ^{230}Th normalized vertical flux. (i) *G. bulloides* $\delta^{18}O$ (Bostock et al., 2015). Age model is from Bostock et al. (2015). Indicated in vertical gray bars are the Holocene (0–12 ka), deglacial (12–18 ka), LGM (18–27 ka), and glacial (27–30 ka) periods. Errors shown for Sr, Nd, and Pb isotopic data are the larger value of the internal or external measured error, and if not shown, the error is smaller than symbol size.

outwash plains. In general, the combined Pb-Sr-Nd data agree with the composition of Australian and New Zealand sources (Figure 4), although there are differences between cores and between LGM and Holocene samples. The most northern core (P71) has isotopic compositions that are consistent with an Australian

source, whereas most of the samples from core TAN1106-28 are more consistent with a New Zealand source (with the exception of a single deglacial sample whose Pb composition suggests a shift to an Australian source). Cores MD97-2121 and TAN1106-43 have isotopic compositions that are consistent with both an Australian source and a New Zealand source. Although our samples also have Pb-Sr-Nd isotopic compositions consistent with a South American source, in atmospheric transport models there is never a significant flux of South American dust to the South Pacific in the Holocene or at the LGM; in both cases the South Pacific is dominated by Australian dust sources (Albani et al., 2012; Li et al., 2008), and thus, it seems likely that any South American contribution to our cores would be minimal. Source regions are generally well sampled for Sr-Nd isotopes, though for Pb isotopes New Zealand and South Africa are poorly sampled (both have only three measurements). As our Sr-Nd and Pb isotope data are in agreement with each other this does not appear to affect our interpretations.

Within a given core there are substantive differences between the isotopic composition in LGM and Holocene sediment. Based on the Nd and Sr isotopic data, the two northernmost cores in our transect (MD97-2121 and P71) have a more continental-like source region (higher $^{87}Sr/^{86}Sr$ and lower ε_{Nd} values) at the LGM relative to the Holocene (Figure 4). In MD97-2121 the higher proportion of fine-grained material and higher detrital flux during the LGM, together with the more continental-like provenance of material, suggests a larger glacial dust flux of Australian origin relative to the Holocene. An increase in Australian dust at the LGM has also been found in sediment cores in the Tasman Sea (De Deckker et al., 2010; Hesse, 1994; Hesse & McTainsh, 2003; Kohfeld et al., 2013; Thiede, 1979) and ice cores recovered from Antarctica (Gili et al., 2016; Revel-Rolland et al., 2006). These studies suggest weakened monsoon rains and expansion of the desert terrains led to an increase in the flux of Australian dust to the SW Pacific at the LGM (Hesse & McTainsh, 2003). In P71 grain size was not measured, but detrital flux from ^{232}Th is slightly lower in the glacial relative to the Holocene (Figure 3). However, P71 was inadvertently sampled prior to the LGM, so this study may not have captured the maximum flux at this site.

In contrast, the glacial sediments in the two southernmost cores, TAN1106-28 and TAN1106-43, have lower $^{87}Sr/^{86}Sr$ and higher ε_{Nd} which indicates a greater proportion of material from a younger, more volcanogenic, source (or a lower proportion of older, more continental material) at the LGM. The Pb isotope results also show that in contrast to the LGM samples, the isotopic composition of Holocene sediments in TAN1106-43 and a deglacial sample from TAN1106-28 are more consistent with Australian sources. These results, combined with the higher dust flux at the LGM (Figure 3), are interpreted as an increase in local, fine-grained material delivered atmospherically or fluvially, from New Zealand at the LGM compared to the Holocene. This higher flux of fine grained material from New Zealand is likely related to greater glacial activity which produced large amounts of very fine glacial till at the LGM (Barrell, 2011). Glaciers in New Zealand were extensive over the South Island at the LGM, but not on the North Island (Barrell, 2011), explaining the different changes in provenance across the latitudinal transect.

In the Atlantic sector of the Southern Ocean and in Antarctic ice cores, the flux of Patagonian dust is substantially higher at the LGM relative to the Holocene (Aarons et al., 2017; Albani et al., 2012; Basile et al., 1997; Delmonte et al., 2017; Neff & Bertler, 2015; Revel-Rolland et al., 2006). These higher dust fluxes in the Atlantic sector of the Southern Ocean are hypothesized to be due to the presence of large glaciers in South America. Glaciers produce vast quantities of very fine grained particles which are transported to their outwash plains where the lack of vegetation and high proportion of fine-grained particles means they are easily mobilized by winds (Bullard et al., 2016; Sugden et al., 2009; Winckler et al., 2008). During the LGM, glaciers covered a large portion of the South Island of New Zealand but were not extensive on the North Island (Barrell, 2011; McGlone et al., 2010). Thus, we propose the same mechanism for the increase in fine-grained material at sites TAN1106-28 and TAN1106-43 at the LGM from New Zealand, albeit to a lesser extent due to the smaller area covered by the glaciers of the New Zealand Southern Alps (Barrell, 2011). This scenario also has implications for the bioavailability of Fe delivered to the South West Pacific at the LGM. The speciation of Fe varies between products of different weathering regimes, leading to a difference in Fe solubility and bioavailability (Schroth et al., 2009). Glacial sources have been found to have a higher Fe solubility and bioavailability, so dust produced by glacial activity in New Zealand could alleviate Fe limitation more effectively than dust produced in arid regimes like Australia (Schroth et al., 2009; Shoenfelt et al., 2018; Yamamoto et al., 2019).
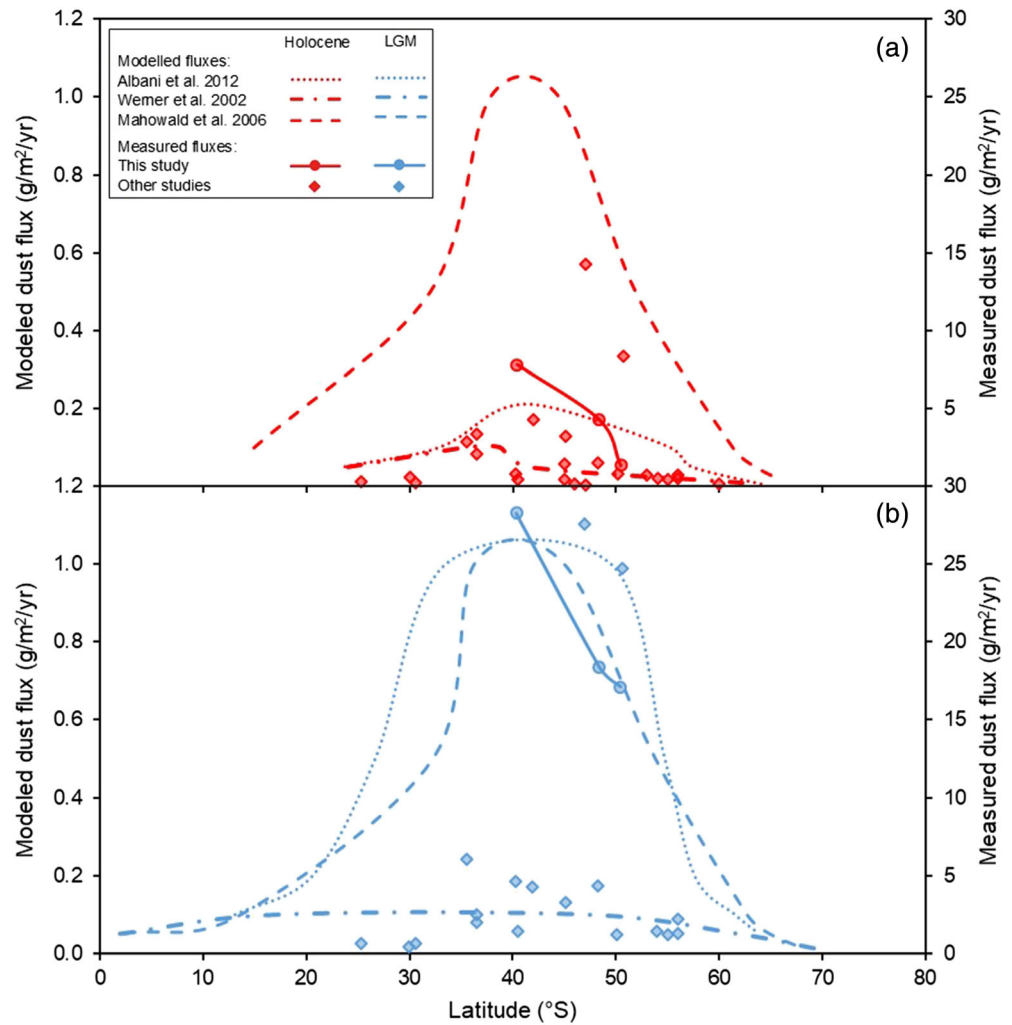
Figure 6. Comparison of average dust flux measured from [232]Th flux in SW Pacific cores in Holocene (a) and LGM (b) age samples to latitudinal transect of modeled dust during the Holocene and LGM at 172°E (Albani et al., 2012; Mahowald et al., 2006; Werner et al., 2002) and other proxy based dust estimates for the SW Pacific (Chase et al., 2003; Durand et al., 2017; Kohfeld et al., 2013; Lambert et al., 2012; Lamy et al., 2014; Marx et al., 2009; Measures & Vink, 2000; Sayles et al., 2001). Transect indicated in Figure 1 by dashed line.

4.3. Discrepancies Between Modeled and Measured Dust Fluxes

Dust flux has previously been modeled for the Holocene and LGM (Albani et al., 2012; Mahowald et al., 2006; Werner et al., 2002). By taking a latitudinal transect at 172°E for the Holocene and LGM from these models and comparing to the latitudinal variation in dust flux measured in the SW Pacific cores in this study, we observe a similar shaped profile (Figure 6). The major difference between modeled and measured dust fluxes is that our observed fluxes are ~25 times higher. Other studies measuring detrital flux from U-series isotopes in the SW Pacific also find higher dust fluxes than those found in models (Anderson et al., 2009; Bradtmiller et al., 2009; Chase et al., 2003; Kohfeld et al., 2013; Lamy et al., 2014), though by less than 1 order of magnitude. This discrepancy between our estimates of dust flux and other measurements of detrital flux is likely because the cores of this study are more proximal to New Zealand, whereas the other studies used cores that are more distal in the Pacific or in the Tasman Sea (Kohfeld et al., 2013; Lamy et al., 2014). As a result, our dust fluxes may also contain a contribution from fluvially delivered material and are not best placed to validate models in the region. Nonetheless, our provenance data still provide useful insights into the origin of this data-model mismatch in that our provenance data indicate an increase in local material

from New Zealand, some of which was likely atmospherically delivered. If New Zealand were an additional, under considered source of dust at the LGM, it may help to explain why models underestimate dust flux at the LGM in this region.

4.4. Timing of Changes

The Sr and Nd isotopes in TAN1106-28 indicate that the changes in provenance occur at the start of the deglaciation, from a more volcanic source at the LGM (average LGM $^{87}Sr/^{86}Sr$: 0.70819, ε_{Nd}: −4.44) to a more continental source during the deglaciation after ~19 ka (average Holocene $^{87}Sr/^{86}Sr$: 0.70870, ε_{Nd}: −4.79, Figure 5). This change in provenance may be related to the rapid retreat of the New Zealand glaciers at the end of the LGM and start of the deglaciation (Bostock et al., 2015; Putnam et al., 2010). The change in provenance occurs prior to the decline in the dust flux, which is more gradual (over ~10 kyr, compared to over ~2 kyr); therefore, it is probable that the changes in provenance were driven by more than simply a change in the relative proportions of the different modes of sediment delivery. The transitional decline in dust flux negatively correlates with the $\delta^{18}O$ record of the core (Figure 5; Bostock et al., 2015) and matches the record of dust flux in the EPICA Dome C ice core (Figure 5, Lambert et al., 2012). The dust in the Antarctic ice cores is thought to be primarily glacial dust from Patagonia (Albani et al., 2012; Basile et al., 1997; Delmonte et al., 2017; Neff & Bertler, 2015; Revel-Rolland et al., 2006), which, as discussed previously, is not likely to reach our cores. However, the consistent timing of dust flux changes supports a similar forcing mechanism, where dust supply is shut off as glaciers retreat and terminate into lakes and fjords instead of transporting material to outwash plains where material is easily mobilized (Sugden et al., 2009). The detrital fluxes in TAN1106-28 reach Holocene levels at ~15 ka, which is slightly earlier than those calculated from ^{232}Th fluxes by Durand et al. (2017). However, this difference may be due to the low temporal resolution of this study or uncertainties in the age model. Although the lower sampling resolution for MD97-2121, TAN1106-43, and P71 precludes such inferences for these sites, they show the same overall trends as TAN1106-28 and support that this reflects a regional rather than a local signal.

4.5. Impact on Primary Productivity

A higher dust flux at the LGM has been suggested to stimulate primary productivity by alleviating Fe limitation in HNLC zones (Martin et al., 1994), with glacially derived dust more bioavailable than other dust sources (Schroth et al., 2009; Shoenfelt et al., 2018, 2019). Although we find an increase in fine-grained dust, or glacial outwash, delivered to our cores at the LGM, we find no evidence for an associated increase in biological productivity (Figure 3). While at MD97-2121 $CaCO_3$ fluxes are higher at the LGM than in the Holocene, this is likely driven by the northward migration of the highly productive subtropical front at the LGM, which is thought to have led to incursions of macronutrient-rich, Fe-poor subantarctic water mixing with the macronutrient-poor Fe-rich subtropical waters at MD97-2121 (Bostock et al., 2015; Carter & Manighetti, 2006; Nelson et al., 2000). At P71, TAN1106-28, and TAN1106-43, our $CaCO_3$ flux records show lower productivity at the LGM compared to the Holocene (Figure 3). This fits with the trend seen in other productivity records from the SW Pacific (C_{org}, excess Ba and opal mass accumulation rates, Zn/Si ratios of sponge spicules; Figure 3, Carter et al., 2000; Chase et al., 2003; Durand et al., 2017; Ellwood et al., 2005), where the only evidence for increased productivity at the LGM is associated with the migration of the highly productive subtropical front (Bostock et al., 2015; Carter & Manighetti, 2006; Durand et al., 2017; Kowalski & Meyers, 1997).

During the LGM and early deglacial, the subtropical front was positioned further north, and thus, TAN1106-28 would have been situated in subantarctic waters, which today are Fe poor and macronutrient rich (Bostock et al., 2015; Carter & Manighetti, 2006). Our record of dust flux from TAN1106-28 shows a decrease by almost a factor of 2 between the LGM and the early deglacial (19–17 ka), but our productivity record ($CaCO_3$ flux) over this time interval remains constant (Figure 3). Alternatively, carbonate flux may not reflect changes in other types of productivity. However, as stated previously there is also little change in the opal flux between the Holocene and LGM (Bostock et al., 2015; Carter & Manighetti, 2006; Durand et al., 2017). Thus, the higher dust fluxes at the LGM do not appear to stimulate productivity in this region, suggesting either the Fe in the lithogenic material was not readily bioavailable or Fe was not the only limiting factor on primary productivity in the Subantarctic Zone of the SW Pacific at the LGM. For instance, the major nutrient content, for example, Si, of the SW Pacific Subantarctic Zone may have been limiting during

the LGM (Boyd et al., 1999; Durand et al., 2017; Moore et al., 2013). Previous work has investigated whether dust might be an important source of Si to the oceans, but as the supply of Si from dust is relatively small compared to riverine and upwelling of deep waters, the changes in dust flux would not contribute much to the Si budget in this region (Tréguer & De La Rocha, 2013). The increased terrestrial flux to the SW Pacific found here without a concomitant increase in biological productivity has implications for the glacial Fe-fertilization hypothesis, indicating that the impact of increased dust on biological productivity was heterogeneous across the Southern Ocean. As a consequence, models that suggest a uniform increase in biological activity likely significantly overestimate the magnitude of CO_2 drawdown by this mechanism.

5. Conclusions

We found a higher flux of fine grained terrestrial material at the LGM compared to the Holocene in four cores from the SW Pacific. In the two most northern cores, the ε_{Nd} and $^{87}Sr/^{86}Sr$ ratios show a more continental signature at the LGM, indicating the glacial increase in lithogenic material came from Australia. The southern cores show a younger, more volcanogenic isotopic signature at the LGM, suggesting that the increase in terrestrial flux is likely driven by more local material derived from New Zealand. We suggest that this increase in local fine-grained material from New Zealand at the LGM is due to the enhanced physical erosion from glacial advance, which provides an additional source of fine-grained, unconsolidated sediment, easily mobilized by wind.

Our finding that Australia provided the increased glacial dust flux to the more northerly MD97-2121 and P71 cores, whereas the glacial increase in the proportion of dust size particles to the more southerly TAN1106-28 and TAN1106-43 cores was from local fine-grained glacial material from New Zealand, highlights the spatial differences in the sources that appear to have nearly ubiquitously enhanced the dust flux throughout the Southern Ocean during the LGM. Consideration of this heterogeneity in dust sources is needed to more accurately model the changes in dust flux in the past. Despite the increase in glacial-induced terrestrial material to the subantarctic SW Pacific, we find little evidence for this leading to increased productivity (e.g., increased biogenic carbonate or opal) in our sites or elsewhere, which indicates that other factors were limiting productivity here at the LGM. This suggests current modeled estimates of the impact of glacial Fe-fertilization of the Southern Ocean on atmospheric CO_2 drawdown are likely maxima.

Data Availability Statement

Data sets are available in the repository PANGAEA (https://doi.pangaea.de/10.1594/PANGAEA.924765).

References

Aarons, S. M., Aciego, S. M., Arendt, C. A., Blakowski, M. A., Steigmeyer, A., Gabrielli, P., et al. (2017). Dust composition changes from Taylor Glacier (East Antarctica) during the last glacial-interglacial transition: A multi-proxy approach. *Quaternary Science Reviews*, *162*, 60–71. https://doi.org/10.1016/j.quascirev.2017.03.011

Albani, S., Mahowald, N. M., Delmonte, B., Maggi, V., & Winckler, G. (2012). Comparing modelled and observed changes in mineral dust transport and deposition to Antarctica between the Last Glacial Maximum and current climates. *Climate Dynamics*, *38*(9–10), 1731–1755. https://doi.org/10.1007/s00382-011-1139-5

Anderson, R. F., Ali, S., Bradtmiller, L. I., Nielsen, S. H. H., Fleisher, M. Q., Anderson, B. E., & Burckle, L. H. (2009). Wind-driven upwelling in the Southern Ocean and the deglacial rise in atmospheric CO_2. *Science*, *323*(5920), 1443–1448. https://doi.org/10.1126/science.1167441

Archer, D., Winguth, A., Lea, D., & Mahowald, N. (2000). What caused the glacial/interglacial atmospheric pCO_2 cycles? *Reviews of Geophysics*, *38*(2), 159–189. https://doi.org/10.1029/1999RG000066

Ardyna, M., Lacour, L., Sergi, S., D'Ovidio, F., Sallée, J. B., Rembauville, M., et al. (2019). Hydrothermal vents trigger massive phytoplankton blooms in the Southern Ocean. *Nature Communications*, *10*(1), 2451. https://doi.org/10.1038/s41467-019-09973-6

Barrell, D. J. A. (2011). Quaternary glaciers of New Zealand. In J. Ehlers, P. L. Gibbard, & P. D. Hughes (Eds.), *Quaternary glaciations— Extent and chronology: A closer look* (pp. 1047–1064). Amsterdam, The Netherlands: Elsevier. https://doi.org/10.1016/B978-0-444-53447-7.00075-1

Basile, I., Grousset, F. E., Revel, M., Petit, J. R., Biscaye, P. E., & Barkov, N. I. (1997). Patagonian origin of glacial dust deposited in East Antarctica (Vostok and Dome C) during glacial stages 2, 4 and 6. *Earth and Planetary Science Letters*, *146*(3–4), 573–589. https://doi.org/10.1016/S0012-821X(96)00255-5

Basile, I., Petit, J. R., Touron, S., Grousset, F. E., & Barkov, N. (2001). Volcanic layers in Antarctic (Vostok) ice cores: Source identification and atmospheric implications. *Journal of Geophysical Research*, *106*(D23), 31,915–31,931. https://doi.org/10.1029/2000JD000102

Bereiter, B., Eggleston, S., Schmitt, J., Nehrbass-Ahles, C., Stocker, T. F., Fischer, H., et al. (2015). Revision of the EPICA Dome C CO_2 record from 800 to 600 kyr before present. *Geophysical Research Letters*, *42*, 542–549. https://doi.org/10.1002/2014GL061957

Bhatia, M. P., Kujawinski, E. B., Das, S. B., Breier, C. F., Henderson, P. B., & Charette, M. A. (2013). Greenland meltwater as a significant and potentially bioavailable source of iron to the ocean. *Nature Geoscience*, *6*(4), 274–278. https://doi.org/10.1038/ngeo1746

Blakowski, M. A., Aciego, S. M., Delmonte, B., Baroni, C., Salvatore, M. C., & Sims, K. W. W. (2016). A Sr-Nd-Hf isotope characterization of dust source areas in Victoria Land and the McMurdo Sound sector of Antarctica. *Quaternary Science Reviews*, *141*, 26–37. https://doi.org/10.1016/j.quascirev.2016.03.023

Blott, S. J., Croft, D. J., Pye, K., Saye, S. E., & Wilson, H. E. (2004). Particle size analysis by laser diffraction. (K. Pye & D. J. Croft, Eds.), *Forensic geoscience: Principles, techniques and applications*. London: The Geological Society of London. Retrieved from http://sp.lyellcollection.org/, 232(1), 63, 73, https://doi.org/10.1144/GSL.SP.2004.232.01.08

Bostock, H. C., Hayward, B. W., Neil, H. L., Sabaa, A. T., & Scott, G. H. (2015). Changes in the position of the subtropical front south of New Zealand since the last glacial period. *Paleoceanography*, *30*, 824–844. https://doi.org/10.1002/2014PA002652

Bostock, H. C., Prebble, J. G., Cortese, G., Hayward, B., Calvo, E., Quirós-Collazos, L., et al. (2019). Paleoproductivity in the SW Pacific Ocean during the early Holocene climatic optimum. *Paleoceanography and Paleoclimatology*, *34*(4), 580–599. https://doi.org/10.1029/2019PA003574

Boyd, P., Laroche, J., Gall, M., Frew, R., & Mckay, R. M. L. (1999). Role of iron, light, and silicate in controlling algal biomass in subantarctic waters SE of New Zealand. *Journal of Geophysical Research*, *104*(C6), 13,395–13,408. https://doi.org/10.1029/1999JC900009

Bradtmiller, L. I., Anderson, R. F., Fleisher, M. Q., & Burckle, L. H. (2009). Comparing glacial and Holocene opal fluxes in the Pacific sector of the Southern Ocean. *Paleoceanography*, *24*, PA2214. https://doi.org/10.1029/2008PA001693

Brown, J. R., Taylor, R. N., & Iguchi, M. (2020). Using high-resolution Pb isotopes to unravel the petrogenesis of Sakurajima volcano, Japan. *Bulletin of Volcanology*, *82*(5), 36. https://doi.org/10.1007/s00445-020-1371-0

Bullard, J. E., Baddock, M., Bradwell, T., Crusius, J., Darlington, E., Gaiero, D. M., et al. (2016). High latitude dust in the Earth system. *Reviews of Geophysics*, *54*, 447–485. https://doi.org/10.1002/2016RG000518

Carter, L., & Manighetti, B. (2006). Glacial/interglacial control of terrigenous and biogenic fluxes in the deep ocean off a high input, collisional margin: A 139 kyr-record from New Zealand. *Marine Geology*, *226*(3–4), 307–322. https://doi.org/10.1016/j.margeo.2005.11.004

Carter, L., Manighetti, B., Ganssen, G., & Northcote, L. (2008). Southwest Pacific modulation of abrupt climate change during the Antarctic Cold Reversal-Younger Dryas. *Palaeogeography, Palaeoclimatology, Palaeoecology*, *260*(1–2), 284–298. https://doi.org/10.1016/j.palaeo.2007.08.013

Carter, L., Neil, H. L., & McCave, I. N. (2000). Glacial to interglacial changes in non-carbonate and carbonate accumulation in the SW Pacific Ocean, New Zealand. *Palaeogeography, Palaeoclimatology, Palaeoecology*, *162*(3–4), 333–356. https://doi.org/10.1016/S0031-0182(00)00137-1

Chase, Z., Anderson, R. F., Fleisher, M. Q., & Kubik, P. W. (2003). Accumulation of biogenic and lithogenic material in the Pacific sector of the Southern Ocean during the past 40,000 years. *Deep Sea Research, Part II*, *50*(3–4), 799–832. https://doi.org/10.1016/S0967-0645(02)00595-7

Costa, K. M., Hayes, C. T., Anderson, R. F., Pavia, F. J., Bausch, A., Deng, F., et al. (2020). ^{230}Th normalization: New insights on an essential tool for quantifying sedimentary fluxes in the modern and Quaternary ocean. *Paleoceanography and Paleoclimatology*, *35*(2), e2019PA003820. https://doi.org/10.1029/2019PA003820

De Angelis, M., Barkov, N. I., & Petrov, V. N. (1987). Aerosol concentrations over the last climatic cycle (160 kyr) from an Antarctic ice core. *Nature*, *325*(6102), 318–321. https://doi.org/10.1038/325318a0

De Deckker, P. (2019). An evaluation of Australia as a major source of dust. *Earth-Science Reviews*, *194*, 536–567. https://doi.org/10.1016/j.earscirev.2019.01.008

De Deckker, P., Norman, M., Goodwin, I. D., Wain, A., & Gingele, F. X. (2010). Lead isotopic evidence for an Australian source of aeolian dust to Antarctica at times over the last 170,000 years. *Palaeogeography, Palaeoclimatology, Palaeoecology*, *285*(3–4), 205–223. https://doi.org/10.1016/j.palaeo.2009.11.013

Delmonte, B., Basile-Doelsch, I., Petit, J. R., Maggi, V., Revel-Rolland, M., Michard, A., et al. (2004a). Comparing the Epica and Vostok dust records during the last 220,000 years: Stratigraphical correlation and provenance in glacial periods. *Earth-Science Reviews*, *66*(1–2), 63–87. https://doi.org/10.1016/j.earscirev.2003.10.004

Delmonte, B., Paleari, C. I., Andò, S., Garzanti, E., Andersson, P. S., Petit, J. R., et al. (2017). Causes of dust size variability in central East Antarctica (Dome B): Atmospheric transport from expanded South American sources during Marine Isotope Stage 2. *Quaternary Science Reviews*, *168*, 55–68. https://doi.org/10.1016/j.quascirev.2017.05.009

Delmonte, B., Petit, J. R., Andersen, K. K., Basile-Doelsch, I., Maggi, V., & Lipenkov, V. Y. (2004b). Dust size evidence for opposite regional atmospheric circulation changes over east Antarctica during the last climatic transition. *Climate Dynamics*, *23*(3–4), 427–438. https://doi.org/10.1007/s00382-004-0450-9

Duncan, B., Carter, L., Dunbar, G. B., Bostock, H. C., Neil, H., Scott, G., et al. (2016). Interglacial/glacial changes in coccolith-rich deposition in the SW Pacific Ocean: An analogue for a warmer world? *Global and Planetary Change*, *144*, 252–262. https://doi.org/10.1016/j.gloplacha.2016.08.001

Durand, A., Chase, Z., Noble, T. L., Bostock, H., Jaccard, S. L., Kitchener, P., et al. (2017). Export production in the New-Zealand region since the Last Glacial Maximum. *Earth and Planetary Science Letters*, *469*, 110–122. https://doi.org/10.1016/j.epsl.2017.03.035

Ellwood, M. J., Kelly, M., Neil, H., & Nodder, S. D. (2005). Reconstruction of paleo-particulate organic carbon fluxes for the Campbell Plateau region of southern New Zealand using the zinc content of sponge spicules. *Paleoceanography*, *20*, PA3010. https://doi.org/10.1029/2004PA001095

Gili, S., Gaiero, D. M., Goldstein, S. L., Chemale, F., Jweda, J., Kaplan, M. R., et al. (2017). Glacial/interglacial changes of Southern Hemisphere wind circulation from the geochemistry of South American dust. *Earth and Planetary Science Letters*, *469*, 98–109. https://doi.org/10.1016/j.epsl.2017.04.007

Gili, S., Gaiero, D. M., Goldstein, S. L., Chemale, F., Koester, E., Jweda, J., et al. (2016). Provenance of dust to Antarctica: A lead isotopic perspective. *Geophysical Research Letters*, *43*, 2291–2298. https://doi.org/10.1002/2016GL068244

Graham, I. J., Glasby, G. P., & Churchman, G. J. (1997). Provenance of the detrital component of deep-sea sediments from the SW Pacific ocean based on mineralogy, geochemistry and Sr isotopic composition. *Marine Geology*, *140*(1–2), 75–96. https://doi.org/10.1016/S0025-3227(97)00006-6

Grousset, F. E., Biscaye, P. E., Revel, M., Petit, J. R., Pye, K., Joussaume, S., & Jouzel, J. (1992). Antarctic (Dome C) ice-core dust at 18 k.y. B.P.: Isotopic constraints on origins. *Earth and Planetary Science Letters*, *111*(1), 175–182. https://doi.org/10.1016/0012-821X(92)90177-W

Haddadchi, A., Booker, D. J., & Measures, R. J. (2017). Predicting river bed substrate cover proportions across New Zealand. *Catena*, *163*, 130–146. https://doi.org/10.1016/j.catena.2017.12.014

Hawkings, J. R., Benning, L. G., Raiswell, R., Kaulich, B., Araki, T., Abyaneh, M., et al. (2018). Biolabile ferrous iron bearing nanoparticles in glacial sediments. *Earth and Planetary Science Letters*, *493*, 92–101. https://doi.org/10.1016/j.epsl.2018.04.022

Hawkings, J. R., Wadham, J. L., Tranter, M., Raiswell, R., Benning, L. G., Statham, P. J., et al. (2014). Ice sheets as a significant source of highly reactive nanoparticulate iron to the oceans. *Nature Communications*, *5*(1), 3929. https://doi.org/10.1038/ncomms4929

Henderson, G. M., & Anderson, R. F. (2003). The U-series toolbox for paleoceanography. *Reviews in Mineralogy and Geochemistry*, *52*(1), 493–531. https://doi.org/10.2113/0520493

Hesse, P. P. (1994). The record of continental dust in Tasman Sea sediments. *Quaternary Science Reviews*, *13*(3), 257–272. https://doi.org/10.1016/0277-3791(94)90029-9

Hesse, P. P., & McTainsh, G. H. (1999). Last glacial maximum to early Holocene wind strength in the mid-latitudes of the Southern Hemisphere from aeolian dust in the Tasman Sea. *Quaternary Research*, *52*(3), 343–349. https://doi.org/10.1006/qres.1999.2084

Hesse, P. P., & McTainsh, G. H. (2003). Australian dust deposits: Modern processes and the Quaternary record. *Quaternary Science Reviews*, *22*(18–19), 2007–2035. https://doi.org/10.1016/S0277-3791(03)00164-1

Hoffmann, D. L., Prytulak, J., Richards, D. A., Elliott, T., Coath, C. D., Smart, P. L., & Scholz, D. (2007). Procedures for accurate U and Th isotope measurements by high precision MC-ICPMS. *International Journal of Mass Spectrometry*, *264*(2–3), 97–109. https://doi.org/10.1016/j.ijms.2007.03.020

Jacobsen, S. B., & Wasserburg, G. J. (1980). Sm-Nd isotopic evolution of chondrites. *Earth and Planetary Science Letters*, *50*(1), 139–155. https://doi.org/10.1016/0012-821X(80)90125-9

Jickells, T. D., An, Z. S., Andersen, K. K., Baker, A. R., Bergametti, C., Brooks, N., et al. (2005). Global iron connections between desert dust, ocean biogeochemistry, and climate. *Science*, *308*(5718), 67–71. https://doi.org/10.1126/science.1105959

Jochum, K. P., Nohl, U., Herwig, K., Lammel, E., Stoll, B., & Hofmann, A. W. (2007). GeoReM: A new geochemical database for reference materials and isotopic standards. *Geostandards and Geoanalytical Research*, *29*(3), 333–338. https://doi.org/10.1111/j.1751-908X.2005.tb00904.x

Kalnay, E., Kanamitsu, M., Kistler, R., Collins, W., Deaven, D., Gandin, L., et al. (1996). The NCEP/NCAR 40-year reanalysis project. *Bulletin of the American Meteorological Society*, *77*(3), 437–471. https://doi.org/10.1175/1520-0477(1996)077<0437:TNYRP>2.0.CO;2

Kohfeld, K. E., Graham, R. M., de Boer, A. M., Sime, L. C., Wolff, E. W., Le Quéré, C., & Bopp, L. (2013). Southern Hemisphere westerly wind changes during the Last Glacial Maximum: Paleo-data synthesis. *Quaternary Science Reviews*, *68*, 76–95. https://doi.org/10.1016/j.quascirev.2013.01.017

Kohfeld, K. E., & Ridgwell, A. (2009). Glacial-interglacial variability in atmospheric CO_2. In C. le Quéré, & E. S. Saltzman (Eds.), *Surface ocean–lower atmosphere processes* (pp. 251–286). Washington DC: American Geophysical Union. https://doi.org/10.1029/2008GM000845

Kowalski, E. A., & Meyers, P. A. (1997). Glacial-interglacial variations in Quaternary production of marine organic matter at DSDP Site 594, Chatham Rise, southeastern New Zealand margin. *Marine Geology*, *140*(3–4), 249–263. https://doi.org/10.1016/S0025-3227(97)00044-3

Kumar, N., Anderson, R. F., Mortlock, R. A., Froelich, P. N., Kubik, P., Dittrich-Hannen, B., & Suter, M. (1995). Increased biological productivity and export production in the glacial southern ocean. *Nature*, *378*(6558), 675–680. https://doi.org/10.1038/378675a0

Lambert, F., Bigler, M., Steffensen, J. P., Hutterli, M., & Fischer, H. (2012). Centennial mineral dust variability in high-resolution ice core data from Dome C, Antarctica. *Climate of the Past*, *8*(2), 609–623. https://doi.org/10.5194/cp-8-609-2012

Lamy, F., Gersonde, R., Winckler, G., Esper, O., Jaeschke, A., Kuhn, G., et al. (2014). Increased dust deposition in the Pacific Southern Ocean during glacial periods. *Science*, *343*(6169), 403–407. https://doi.org/10.1126/science.1245424

Lang, D. C., Bailey, I., Wilson, P. A., Beer, C. J., Bolton, C. T., Friedrich, O., et al. (2014). The transition on North America from the warm humid Pliocene to the glaciated Quaternary traced by eolian dust deposition at a benchmark North Atlantic Ocean drill site. *Quaternary Science Reviews*, *93*, 125–141. https://doi.org/10.1016/j.quascirev.2014.04.005

Li, F., Ginoux, P., & Ramaswamy, V. (2008). Distribution, transport, and deposition of mineral dust in the Southern Ocean and Antarctica: Contribution of major sources. *Journal of Geophysical Research*, *113*, D10207. https://doi.org/10.1029/2007JD009190

Lisiecki, L. E., & Raymo, M. E. (2005). A Pliocene-Pleistocene stack of 57 globally distributed benthic δ18O records. *Paleoceanography*, *20*, PA1003. https://doi.org/10.1029/2004PA001071

Maher, B. A., Prospero, J. M., Mackie, D., Gaiero, D. M., Hesse, P. P., & Balkanski, Y. (2010). Global connections between aeolian dust, climate and ocean biogeochemistry at the present day and at the last glacial maximum. *Earth-Science Reviews*, *99*(1–2), 61–97. https://doi.org/10.1016/j.earscirev.2009.12.001

Mahowald, N. M., Baker, A. R., Bergametti, G., Brooks, N., Duce, R. A., Jickells, T. D., et al. (2005). Atmospheric global dust cycle and iron inputs to the ocean. *Global Biogeochemical Cycles*, *19*, GB4025. https://doi.org/10.1029/2004GB002402

Mahowald, N. M., Muhs, D. R., Levis, S., Rasch, P. J., Yoshioka, M., Zender, C. S., & Luo, C. (2006). Change in atmospheric mineral aerosols in response to climate: Last glacial period, preindustrial, modern, and doubled carbon dioxide climates. *Journal of Geophysical Research*, *111*, D10202. https://doi.org/10.1029/2005JD006653

Martin, J. H., Coale, K. H., Johnson, K. S., Fitzwater, S. E., Gordon, R. M., Tanner, S. J., et al. (1994). Testing the iron hypothesis in ecosystems of the equatorial Pacific Ocean. *Nature*, *371*(6493), 123–129. https://doi.org/10.1038/371123a0

Martínez-García, A., Sigman, D. M., Ren, H., Anderson, R. F., Straub, M., Hodell, D. A., et al. (2014). Iron fertilization of the subantarctic ocean during the Last Ice Age. *Science*, *343*(6177), 1347–1350. https://doi.org/10.1126/science.1246848

Marx, S. K., Kamber, B. S., & McGowan, H. A. (2005). Provenance of long-travelled dust determined with ultra-trace-element composition: A pilot study with samples from New Zealand glaciers. *Earth Surface Processes and Landforms*, *30*(6), 699–716. https://doi.org/10.1002/esp.1169

Marx, S. K., Kamber, B. S., McGowan, H. A., Petherick, L. M., McTainsh, G. H., Stromsoe, N., et al. (2018). Palaeo-dust records: A window to understanding past environments. *Global and Planetary Change*, *165*, 13–43. https://doi.org/10.1016/j.gloplacha.2018.03.001

Marx, S. K., McGowan, H. A., & Kamber, B. S. (2009). Long-range dust transport from eastern Australia: A proxy for Holocene aridity and ENSO-type climate variability. *Earth and Planetary Science Letters*, *282*(1–4), 167–177. https://doi.org/10.1016/j.epsl.2009.03.013

McGee, D., Broecker, W. S., & Winckler, G. (2010). Gustiness: The driver of glacial dustiness? *Quaternary Science Reviews*, *29*(17–18), 2340–2350. https://doi.org/10.1016/j.quascirev.2010.06.009

McGee, D., Marcantonio, F., & Lynch-Stieglitz, J. (2007). Deglacial changes in dust flux in the eastern equatorial Pacific. *Earth and Planetary Science Letters*, *257*(1–2), 215–230. https://doi.org/10.1016/j.epsl.2007.02.033

McGlone, M. S., Newnham, R. M., & Moar, N. T. (2010). The vegetation cover of New Zealand during the Last Glacial Maximum: Do pollen records under-represent woody vegetation? In S. G. Haberle, J. Stevenson, M. Prebble (Eds.), *Altered ecologies: Fire, climate and human influence on terrestrial landscapes* (pp. 49–68). Canberra, Australia: ANU E Press. https://doi.org/10.22459/TA32.11.2010.04

Measures, C. I., & Vink, S. (2000). On the use of dissolved aluminum in surface waters to estimate dust deposition to the ocean. *Global Biogeochemical Cycles*, *14*(1), 317–327. https://doi.org/10.1029/1999GB001188

Molina-Kescher, M., Frank, M., & Hathorne, E. C. (2014). Nd and Sr isotope compositions of different phases of surface sediments in the South Pacific: Extraction of seawater signatures, boundary exchange, and detrital/dust provenance. *Geochemistry, Geophysics, Geosystems*, *15*, 3502–3520. https://doi.org/10.1002/2014GC005443

Moore, C. M., Mills, M. M., Arrigo, K. R., Berman-Frank, I., Bopp, L., Boyd, P. W., et al. (2013). Processes and patterns of oceanic nutrient limitation. *Nature Geoscience*, *6*(9), 701–710. https://doi.org/10.1038/ngeo1765

Muhs, D. R., Budahn, J., Reheis, M., Beann, J., Skipp, G., & Fisher, E. (2007). Airborne dust transport to the eastern Pacific Ocean off southern California: Evidence from San Clemente Island. *Journal of Geophysical Research*, *112*, D13203. https://doi.org/10.1029/2006JD007577

Neff, P. D., & Bertler, N. A. N. (2015). Trajectory modeling of modern dust transport to the Southern Ocean and Antarctica. *Journal of Geophysical Research: Atmospheres*, *120*, 9303–9322. https://doi.org/10.1002/2015JD023304

Nelson, C. S., Hendy, I. L., Neil, H. L., Hendy, C. H., & Weaver, P. P. E. (2000). Last glacial jetting of cold waters through the subtropical convergence zone in the Southwest Pacific off eastern New Zealand, and some geological implications. *Palaeogreography, Palaeoclimatology, Palaeoecology*, *156*(1–2), 103–121. https://doi.org/10.1016/S0031-0182(99)00134-0

Nier, A. O. (1938). The isotopic constitution of strontium, barium, bismuth, thallium and mercury. *Physical Review*, *54*(4), 275–278. https://doi.org/10.1103/PhysRev.54.275

Nita, D.C. (2012). Uranium series disequilibrium dating, PhD thesis, Faculty of Environmental Science and Engineering. Babeş-Bolyai University, 1–140.

Paterson, G. A., & Heslop, D. (2015). New methods for unmixing sediment grain size data. *Geochemistry, Geophysics, Geosystems*, *16*, 4494–4506. https://doi.org/10.1002/2015GC006070

Pichat, S., Abouchami, W., & Galer, S. J. G. (2014). Lead isotopes in the Eastern Equatorial Pacific record Quaternary migration of the South Westerlies. *Earth and Planetary Science Letters*, *388*, 293–305. https://doi.org/10.1016/j.epsl.2013.11.035

Pugh, R. S., & McCave, I. N. (2011). Particle size measurement of diatoms with inference of their properties: Comparison of three techniques. *Journal of Sedimentary Research*, *81*(8), 600–610. https://doi.org/10.2110/jsr.2011.43

Putnam, A. E., Denton, G. H., Schaefer, J. M., Barrell, D. J. A., Andersen, B. G., Finkel, R. C., et al. (2010). Glacier advance in southern middle-latitudes during the Antarctic Cold Reversal. *Nature Geoscience*, *3*(10), 700–704. https://doi.org/10.1038/ngeo962

Ramirez, M. T., Allison, M. A., Bianchi, T. S., Cui, X., Savage, C., Schüller, S. E., et al. (2016). Modern deposition rates and patterns of organic carbon burial in Fiordland, New Zealand. *Geophysical Research Letters*, *43*, 11,768–11,776. https://doi.org/10.1002/2016GL070021

Rea, D. K. (1994). The paleoclimatic deposition record provided of wind by eolian in the deep sea: The geologic history of wind. *Reviews of Geophysics*, *32*(2), 159–195. https://doi.org/10.1029/93RG03257

Revel-Rolland, M., De Deckker, P., Delmonte, B., Hesse, P. P., Magee, J. W., Basile-Doelsch, I., et al. (2006). Eastern Australia: A possible source of dust in East Antarctica interglacial ice. *Earth and Planetary Science Letters*, *249*(1–2), 1–13. https://doi.org/10.1016/j.epsl.2006.06.028

Russel, W. A., Papanastassiou, D. A., & Tombrello, T. A. (1978). Ca isotope fractionation on the earth and other solar system materials. *Geochimica et Cosmochimica Acta*, *42*(8), 1075–1090. https://doi.org/10.1016/0016-7037(78)90105-9

Sayles, F. L., Martin, W. R., Chase, Z., & Anderson, R. F. (2001). Benthic remineralization and burial of biogenic SiO_2, $CaCO_3$, organic carbon, and detrital material in the Southern Ocean along a transect at 170° west. *Deep-Sea Research Part II*, *48*(19–20), 4323–4383. https://doi.org/10.1016/S0967-0645(01)00091-1

Scher, H. D., & Delaney, M. L. (2010). Breaking the glass ceiling for high resolution Nd isotope records in early Cenozoic paleoceanography. *Chemical Geology*, *269*(3–4), 329–338. https://doi.org/10.1016/j.chemgeo.2009.10.007

Schroth, A. W., Crusius, J., Sholkovitz, E. R., & Bostick, B. C. (2009). Iron solubility driven by speciation in dust sources to the ocean. *Nature Geoscience*, *2*(5), 337–340. https://doi.org/10.1038/ngeo501

Shoenfelt, E. M., Sun, J., Winckler, G., Kaplan, M. R., Borunda, A. L., Farrell, K. R., et al. (2017). High particulate iron (II) content in glacially sourced dusts enhances productivity of a model diatom. *Science Advances*, *3*(6), e1700314. https://doi.org/10.1126/sciadv.1700314

Shoenfelt, E. M., Winckler, G., Annett, A. L., Hendry, K. R., & Bostick, B. C. (2019). Physical weathering intensity controls bioavailable primary iron (II) silicate content in major global dust sources. *Geophysical Research Letters*, *46*, 10,854–10,864. https://doi.org/10.1029/2019GL084180

Shoenfelt, E. M., Winckler, G., Lamy, F., Anderson, R. F., & Bostick, B. C. (2018). Highly bioavailable dust-borne iron delivered to the Southern Ocean during glacial periods. *Proceedings of the National Academy of Sciences of the United States of America*, *115*(44), 11,180–11,185. https://doi.org/10.1073/pnas.1809755115

Sugden, D. E., McCulloch, R. D., Bory, A. J. M., & Hein, A. S. (2009). Influence of Patagonian glaciers on Antarctic dust deposition during the last glacial period. *Nature Geoscience*, *2*(4), 281–285. https://doi.org/10.1038/ngeo474

Tagliabue, A., Bowie, A., Boyd, P. W., Buck, K. N., Johnson, K. S., & Saito, M. (2017). The integral role of iron in ocean biogeochemistry. *Nature*, *543*(7643), 51–59. https://doi.org/10.1038/nature21058

Tanaka, T., Togashi, S., Kamioka, H., Amakawa, H., Kagami, H., Hamamoto, T., et al. (2000). JNdi-1: A neodymium isotopic reference in consistency with LaJolla neodymium. *Chemical Geology*, *168*(3–4), 279–281. https://doi.org/10.1016/S0009-2541(00)00198-4

Taylor, R. N., Ishizuka, O., Michalik, A., Milton, J. A., & Croudace, I. W. (2015). Evaluating the precision of Pb isotope measurement by mass spectrometry. *Journal of Analytical Atomic Spectrometry*, *30*(1), 198–213. https://doi.org/10.1039/c4ja00279b

Taylor, S. R., & McLennan, S. M. (1985). *The continental crust: Its composition and evolution*. Oxford: Blackwell Science.

Thiede, J. (1979). Wind regimes over the late Quaternary southwest Pacific Ocean. *Geology*, *7*(5), 259–262. https://doi.org/10.1130/0091-7613(1979)7<259:WROTLQ>2.0.CO;2

Tréguer, P. J., & De La Rocha, C. L. (2013). The world ocean silica cycle. *Annual Review of Marine Science*, *5*(1), 477–501. https://doi.org/10.1146/annurev-marine-121211-172346

Vallelonga, P., Gabrielli, P., Balliana, E., Wegner, A., Delmonte, B., Turetta, C., et al. (2010). Lead isotopic compositions in the EPICA Dome C ice core and Southern Hemisphere potential source areas. *Quaternary Science Reviews*, *29*(1–2), 247–255. https://doi.org/10.1016/j.quascirev.2009.06.019

Vance, D., & Thirlwall, M. (2002). An assessment of mass discrimination in MC-ICPMS using Nd isotopes. *Chemical Geology*, *185*(3–4), 227–240. https://doi.org/10.1016/S0009-2541(01)00402-8

Wengler, M., Lamy, F., Struve, T., Borunda, A., Böning, P., Geibert, W., et al. (2019). A geochemical approach to reconstruct modern dust fluxes and sources to the South Pacific. *Geochimica et Cosmochimica Acta*, *264*, 205–223. https://doi.org/10.1016/j.gca.2019.08.024

Werner, M., Tegen, I., Harrison, S. P., Kohfeld, K. E., Prentice, I. C., Balkanski, Y., et al. (2002). Seasonal and interannual variability of the mineral dust cycle under present and glacial climate conditions. *Journal of Geophysical Research*, *107*(D24), 4744. https://doi.org/10.1029/2002JD002365

Winckler, G., Anderson, R. F., Fleisher, M. Q., McGee, D., & Mahowald, N. (2008). Covariant glacial-interglacial dust fluxes in the equatorial Pacific and Antarctica. *Science*, *320*(5872), 93–96. https://doi.org/10.1126/science.1150595

Yamamoto, A., Abe-Ouchi, A., Ohgaito, R., Ito, A., & Oka, A. (2019). Glacial CO_2 decrease and deep-water deoxygenation by iron fertilization from glaciogenic dust. *Climate of the Past*, *15*(3), 981–996. https://doi.org/10.5194/cp-15-981-2019

Yobregat, E., Fitoussi, C., & Bourdon, B. (2017). A new method for TIMS high precision analysis of Ba and Sr isotopes for cosmochemical studies. *Journal of Analytical Atomic Spectrometry*, *32*(7), 1388–1399. https://doi.org/10.1039/C7JA00012J